Quantifying Feedbacks Between Ice Flow, Grain Size, and Basal Meltwater on Annual and Decadal Time-Scales Using a 2-D Ice Sheet Model

Joshua H. Rines

A thesis

submitted to the Faculty of

the department of Earth and Environmental Sciences

in partial fulfillment

of the requirements for the degree of

Master of Science

Boston College
Morrissey College of Arts and Sciences
Graduate School

May 2022

Quantifying Feedbacks Between Ice Flow, Grain Size, and Basal Meltwater on Annual and Decadal Time-Scales Using a 2-D Ice Sheet Model

Joshua H. Rines
Advisor: Professor Mark D. Behn

Ice sheet flow is strongly controlled by the conditions at the ice-bed interface. While these processes are hard to observe directly, comparisons between numerical modeling and ice surface observations can be used to indirectly infer subglacial processes. Specifically, seasonal summer speed up near the margin of the Greenland Ice Sheet (GIS) has been linked to the presence of subglacial water. For decades, the Glen flow law has been the most widely-accepted constitutive relation for modeling ice flow. However, while the Glen law captures the temperature-dependent, nonlinear viscosity of ice, it does not explicitly incorporate ice grain size, which has been shown in laboratory experiments to influence ice rheology. To compensate for the lack of explicit grain size dependence, ice sheet models often utilize an "enhancement factor" that modifies the flow law to better match observations, but does not provide insight into the physical processes at play. Using a grain size sensitive rheology that incorporates grain size evolution due to dynamic recrystallization and grain growth, I model the effects of seasonal variations of subglacial hydrology in a 2-D vertical cross-section of ice flow on both annual and inter-annual timescales. The presence of subglacial water reduces the frictional coupling between the ice and the bed. Here I simulate the presence of water at the ice-bed interface during the melt season using patches of free-slip and explore a range of patch sizes and geometries to investigate their role in modulating ice surface velocities and grain size within the ice. I compare modeled winter and summer surface velocities to observations taken on the western margin of the GIS and find that realistic surface velocities are achievable using a

grain size sensitive flow law without the introduction of an enhancement factor. Further, the grain size of the internal ice responds on an inter-annual timescale to these seasonal forcings at the bed, potentially leading to long-term changes in surface velocities.

Table of Contents

Acknowledgements

Thank you to my advisor, Professor Mark Behn, for his patience, support, guidance, and inspiration through this process. Thank you to Professor Noah Snyder for his helpful reviews on this work and thoughtful guidance throughout.

List of Figures

List of Tables

1. Introduction

The Greenland Ice Sheet (GIS) is losing ice mass at an increasing rate [e.g., *Shepherd et al.*, 2012]. This can be attributed to two coupled processes: surface melt [*van den Broeke et al.*, 2009; *Hanna et al.*, 2013] and the dynamic effect of ice flow into the ocean [*Pritchard et al.*, 2009]. These two processes do not operate independently of one another, rather they are inherently coupled. In summer months, surface meltwater is transported via vertical cracks (e.g., moulins/crevasses) to the bed of the ice sheet [*Das et al.*, 2008; *Doyle et al.*, 2013]. Once at the bed, the water acts as a lubricant, decreasing the frictional coupling between the bed and the ice sheet and dynamically modifying ice flow velocities through the summer melt season [*Zwally et al.*, 2002]. The result is a canonical annual ice flow velocity curve (Figure 1) that is characterized by five main time periods: (1) slow velocities during the winter and spring months, (2) rapid ice flow acceleration in the beginning of the summer melt season, (3) highly variable but decreasing velocities during the summer, (4) a velocity minimum at the conclusion of the summer melt season, and (5) a return to slower winter/spring velocities [*Stevens et al.*, 2016].

A conceptual model of the hydrological evolution beneath the Greenland Ice Sheet during a melt season (Figure 1, top) originates from velocity and hydrological observations of alpine glaciers [c.f. *Fountain & Walder*, 1998]. This model posits that with low meltwater input, such as at the beginning of the melt season, the meltwater present at the bed is distributed in isolated cavities. As the season progresses and the ice-bed interface receives more meltwater, these cavities link together to form a more efficient channelized drainage network. This channelization leads to increased frictional coupling between the ice and the bed, and ultimately a slow-down in ice velocities toward the end of the melt season [e.g., *Schoof*, 2010; *Hewitt*, 2013]. Observed surface velocities (Figure 1, bottom) reflect changes in the basal conditions, as well as the rate of internal ice deformation. Further, temporal and spatial variations in basal conditions influence stress and strain rate within the ice sheet, producing a feedback with the nonlinear rheology of the internal ice. It is thus necessary to constrain these feedbacks between ice-bed boundary conditions and internal ice deformation in order to understand and predict the flow of the GIS.

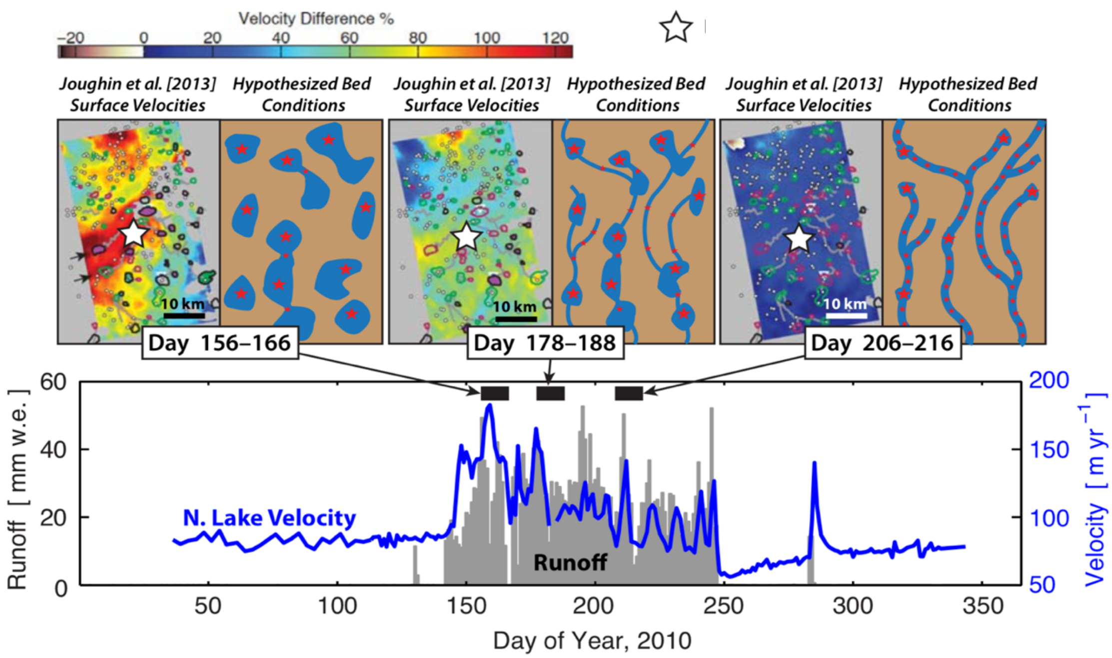

Figure 1. Top: Hypothesized evolution of subglacial meltwater system over the summer season compared to 13-day surface velocities from *Joughin et al.* [2013]. **Bottom:** Idealized annual ice velocity curve from [*Stevens et al.*, 2016]. The blue curve depicts ice surface speed and the grey curve depicts the annual meltwater runoff evolution.

On the ice sheet scale, the GIS deforms in response to the vertical gravitational force. Gravity sets the stress gradients throughout an ice mass, driving deformation characterized by solid-state viscous creep. Phenomenologically, an ice sheet will spread over a relatively flat bed in a similar way as honey or molasses would spread out if poured onto a table top. The flow of ice is typically characterized by the constitutive power law relation known as the Glen flow law. The Glen law relates stress (σ) and strain rate ($\dot{\varepsilon}$) as

$$\dot{\varepsilon} = B\sigma^n, \qquad (1)$$

where B is a temperature-dependent constant that captures the Arrhenius nature of creep, and n is termed the stress exponent. The Glen law has a characteristic stress exponent of $n \sim 3$, experimentally derived from laboratory experiments on polycrystalline ice [*Glen*, 1952; 1955]. Several studies have supported the Glen law's efficacy in describing natural ice flow in glaciers and ice sheets [e.g., *Weertman*, 1983]. For example, *Paterson* [1983] used borehole tilt measurements in ice sheets to show that the relationship between stress and strain rate was consistent with a n ~ 3 rheology. However, despite the fact that the Glen law has been widely used to describe the creep of ice masses, field and laboratory experiments suggest that it may be an oversimplification of ice rheology over a broad range of stresses, where ice flow may be more accurately described by stress exponents of $n \neq 3$ [e.g., *Goldsby and Kohlstedt*, 2001; *Millstein et al.*, 2021]. Specifically, *Goldsby & Kohlstedt* [2001] found that the stress exponent is dependent on the grain size of the ice crystals, an effect which is often parameterized via an enhancement factor. Enhancement factors are commonly introduced into ice flow models in an attempt to approximate ice properties, such as grain size, to allow for better match between observations and models. These enhancement factors modify the prefactor, B, in the Glen law [e.g., *Luthi et al.*, 2002; *Cuffey & Paterson*, 2010].

In particular, lab experiments by *Goldsby & Kohlstedt* [2001] demonstrated that the stress exponent deviates from $n \sim 3$ in high and low stress regimes, with a stress exponent

n = 4 at high stresses and n =1.8 at low stresses (Figure 2). The high-stress, high-n regime indicates a grain size-independent flow via the dislocation creep mechanism. The low-stress low-n regime reflects a dependence on grain size and reflects grain boundary sliding (GBS) creep mechanism. GBS mechanisms are described by an increase in strain rate with decreasing grain size, i.e., $\dot{\varepsilon} \propto d^{-m}$, where d is grain size and the grain size exponent ranges in value $1 \leq m \leq 3$ depending on the mechanism accommodating the GBS [*Poirier*, 1985]. In this study the grain size exponent is m = 1.4, indicative of dislocation-accommodated GBS creep [*Nieh et al.*, 1997].

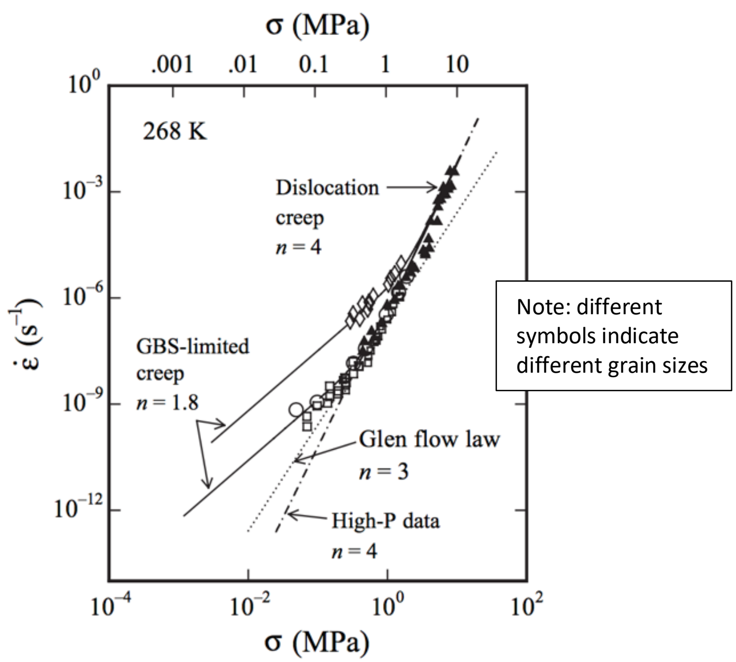

Figure 2. Strain rate versus stress data from *Goldsby & Kohlstedt* [2001] experiments demonstrating the n = 4 dislocation creep and n = 1.8 GBS regimes. The different shaped symbols represent experiments run on samples of different grain size, demonstrating that creep by GBS is grain size dependent, but dislocation creep is not. Specifically, the grain sizes are: d = 0.2 mm (diamonds); d > 1 mm (squares, ircles, triangles). Figure from *Goldsby & Kohlstedt* [2001].

The experiments mentioned above were conducted on polycrystalline samples with grain sizes much smaller (3–200 μm) than typically found in natural ice sheet settings (1–10 mm). By contrast, earlier experiments, including those by *Glen* [1952; 1955], were conducted using crystals on the order of natural grain sizes. But at lab conditions, these grain sizes result in strain rates that are so slow that transient creep will likely dominate [*Weertman*, 1983], obscuring the GBS creep regime. For this reason, *Goldsby & Kohlstedt* [2001] fabricated much smaller crystals (3–200 μm) to gain access to the low-n, GBS regime on laboratory-relevant timescales and without contamination by transient creep.

The n = 1.8 and n = 4 creep regimes in the Goldsby & Kohlstedt [2001] ice deformation experiments would seem to contradict the Glen law assumption that ice deformation can be accurately described by a uniform stress exponent of n = 3. One hypothesis to explain this apparent contradiction is that both creep regimes operate simultaneously, leading to an effective stress exponent similar to that of the Glen flow law [e.g., *Behn et al.*, 2021]. Because the GBS creep mechanism is dependent on grain size, the overall rheology will therefore also be dependent on grain size. Some rheologic descriptions of ice have taken grain size into account, such as *Faria et al.* [2014a], where steady-state grain size is a function of temperature and strain rate. However, in this formulation the steady-state grain size was derived based on the grain size-independent Glen law. More recently *Behn et al.* [2021] derived a 1D model of grain size evolution (GSE), based on the "wattmeter" originally developed by *Austin & Evans* [2007] for grain size evolution in solid Earth materials. *Behn et al.* [2021] coupled this grain size evolution model to a composite (i.e., multiple creep mechanisms) flow law that accounts for the experiments of *Goldsby & Kohlstedt* [2001]. However, a fully-coupled grain size evolution-dependent rheology reflecting the two experimentally-determined creep regimes has not yet been implemented into 2-D ice sheet modeling.

Here, I implement a fully-coupled grain size-sensitive rheology into 2-D numerical ice sheet model, building on the work of *Behn et al.* [2021], to explore the effects of grain size on ice sheet flow in regions experiencing seasonally-varying meltwater input at the bed. In particular, I quantify the annual cycle of ice grain size evolution associated with regions of enhanced basal slip, the inter-annual evolution of ice grain size in response to continual seasonal basal boundary condition perturbations, and investigate the influence of these changes on ice sheet flow and surface velocities. These results may have important implications for large-scale ice sheet models that do not yet incorporate self-consistent rheological responses to perturbations in basal boundary conditions.

2. Methods

The goal of this project is to investigate annual and inter-annual variations in ice grain size in response to seasonal perturbations in slip conditions at the ice-bed interface. Below, I describe my approach for simulating ice sheet deformation, incorporating a self-consistent treatment of grain size evolution and grain size sensitive creep. I discuss the importance and mathematics of grain size evolution (§2.1) and how it is integrated with ice rheology in the form of a composite flow law (§2.2). This rheology is expressed as an effective viscosity that I use as a dynamic material parameter in my modeling. I discuss the formulation of the effective viscosity (§2.3) and my numerical implementation (§2.4), and then close the section with a description of the model domain, boundary conditions, and what portion of the GIS the model simulates (§2.5).

2.1 Grain Size Evolution (GSE)

Just as solid Earth materials are comprised of an aggregate of many mineral grains, so too are ice masses composed of small grains of their respective constitutive mineral, ice (Figure 3).

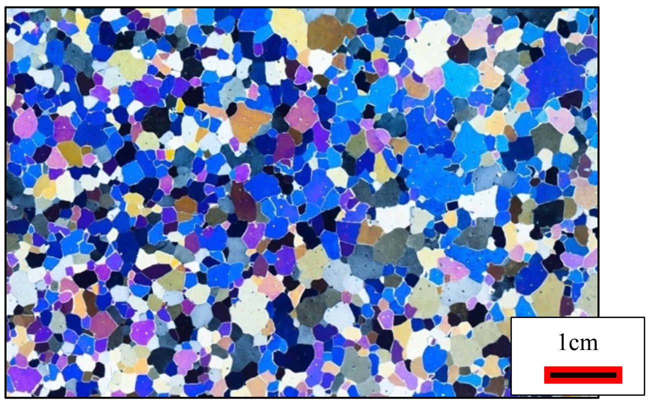

Figure 3. Thin section of ice showing individual grains. From USGS, online.

The temporal evolution of ice grain size is determined by the rate of grain growth and the rate of grain size reduction (recrystallization) [e.g., *Alley*, 1992]. In an ice sheet, grain size typically increases with depth in the upper layers of ice and then decreases with further depth, ranging from roughly 1 mm to 15 mm (Figure 4). In this near the surface domain, grain size evolution is likely dominated by grain growth [*Gow et al*., 1997], while at greater depths recrystallization processes become more prevalent [e.g., *Roessinger et al*., 2011; *Faria et al*., 2014a]. Models of analogous processes in the crust and mantle are successful at predicting grain size evolution in olivine [e.g., *Hall & Parmentier*, 2003, *Austin & Evans*, 2007; 2009]. Finally, there is often a region of large grain sizes near the bottom of the ice core sample (Figure 4). These large grain sizes may be caused by an enhancement in basal ice fabric [*Behn et al.*, 2021] or the effect of migration recrystallization [*Ranganathan et al.*, 2021]. As shown below, grain size evolution in this region is not captured by my model; however, the relatively localized region of large grain size likely has a relatively small influence on my final results. Future work is needed to better understand grain growth kinematics and fabric development in basal ice.

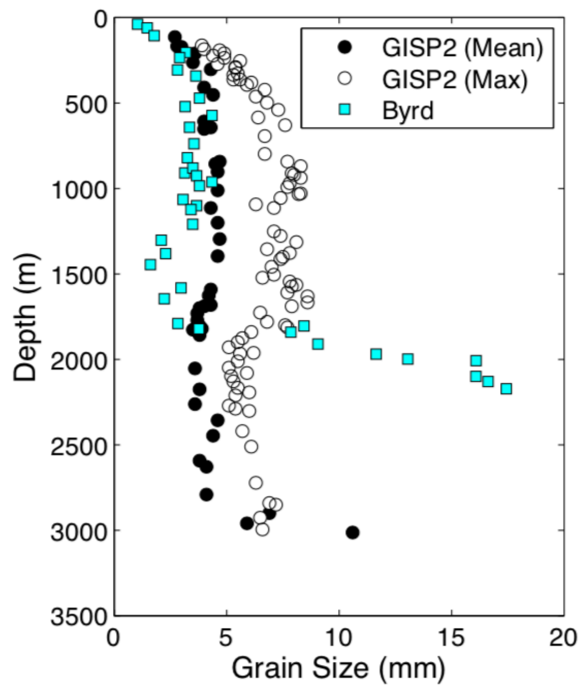

Figure 4. Grain size versus depth in three ice core records. Filled circles are GISP-2 mean grain size [*Alley & Woods*, 1996]; open circles are GISP-2 max grain size [*Gow et al.*, 1997]; blue squares are from Byrd Station [*Gow & Williamson*, 1976].

The grain size evolution model used here is based on *Behn et al*. [2021], who adapted the "wattmeter" [*Austin & Evans*, 2007; 2009], originally formulated to quantify grain size evolution in crustal and mantle rocks. The wattmeter operates on the premise that the change in grain size is controlled by a competition between grain size growth rate and grain size recrystallization rate:

$$\dot{d} = \dot{d}_{gg} - \dot{d}_{red}, \tag{2}$$

where $\dot{d}$ is the time derivative of average grain size, $\dot{d}_{gg}$ is the grain growth rate, and $\dot{d}_{red}$ is the rate of grain size reduction. Grain growth rate follows a standard relation,

$$\dot{d}_{gg} = p^{-1} d^{1-p} K_{gg} \exp\left(-\frac{Q_{gg}}{RT}\right), \tag{3}$$

where R is the universal gas constant, T is temperature, p is the grain growth exponent, K_{gg} is the grain growth constant, and Q_{gg} is the activation enthalpy. The grain growth parameters, p, Q_{gg}, and K_{gg} depend on impurities in the ice [e.g., *Alley et al.*, 1986] and were selected based on a combination of laboratory and ice core data [*Behn et al.*, 2021]. The grain size reduction rate assumed by the wattmeter is dependent on a balance of the mechanical work rate and the rate of work dissipation [*Austin & Evans*, 2007; 2009]. Grain size reduction is given as

$$\dot{d}_{red} = \frac{(\lambda_{GBS} - \beta\lambda_{GBS+}\beta\lambda_{disl})d^2}{-c\gamma} \sigma\dot{\varepsilon}, \tag{4}$$

where λ_{GBS} and λ_{disl} are the fraction of work that increases the internal energy leading to grain size reduction for GBS and dislocation creep, respectively (the rest of the energy is dissipated), β is the ratio of dislocation work rate to total work rate, c is a geometrical factor, and γ is the grain boundary energy. Values for λ_{GBS} and λ_{disl} were estimated by *Behn et al.* [2021] based on comparison to laboratory experiments. Substituting Eq. (3) and Eq. (4) into Eq. (2) gives the full grain size evolution equation:

$$\dot{d}_{total} = p^{-1} d^{1-p} K_{gg} \exp\left(-\frac{Q_{gg}}{RT}\right) - \frac{(\lambda_{GBS} - \beta\lambda_{GBS+}\beta\lambda_{disl})d^2}{-c\gamma} \sigma\dot{\varepsilon}. \tag{5}$$

If $\dot{d}_{total} = 0$, a steady-state grain size can be defined:

$$\dot{d}_{ss}^{1+p} = \frac{K_{gg} \exp\left(-\frac{Q_{gg}}{RT}\right) p^{-1} c\gamma}{(\lambda_{GBS} - \beta\lambda_{GBS+}\beta\lambda_{disl})\sigma\dot{\varepsilon}}. \tag{6}$$

Calculating a steady-state grain size requires an iterative process between the grain size and strain rate. The steady-state grain size is often a useful characterization, but will sometimes not accurately represent the grain size in regions of an ice sheet where the grains have not had sufficient time to equilibrate with their surrounding conditions. These non-steady-state cases require the use of Eq. (5) in conjunction with the constitutive relations to solve for the grain size that is consistent with the evolving stress and strain rate fields. Because I am interested in time-dependent grain size evolution, I use Eq. (5), which is formulated in terms of the second invariant of stress and strain rate for implementation in the numerical model described below.

2.2 Composite Flow Law

As mentioned above, there are two prevalent creep regimes in ice marked by two different stress exponents: GBS creep, operating at lower stresses (n = 1.8), and dislocation creep, operating at higher stresses (n = 4). In my models, I implement a flow law that is a linear combination of the GBS and dislocation creep flow laws:

$$\dot{\varepsilon} = \dot{\varepsilon}_{GBS} + \dot{\varepsilon}_{disl}. \tag{7}$$

Each term on the right is defined by its own independent flow law of the form

$$\dot{\varepsilon}_k = A_k d^{-m_k} \sigma^{n_k} \exp\left(-\frac{Q_k}{RT}\right), \tag{8}$$

where A_k is a material constant, m_k is the grain size exponent, n_k is the stress exponent, Q_k is the activation energy. Terms with a subscript k are specific to each independent flow law (i.e., GBS or dislocation creep). For example, because dislocation creep is grain size-insensitive, m_{disl} = 0. Each of these flow laws are formulated in terms of the second invariants. Because the flow laws (Eq. 8) and the grain size evolution equation (Eq. 5) are coupled through grain size and stress, they must be solved iteratively (see §2.4 below). The flow parameters for GBS and dislocation creep are taken from *Goldsby & Kohlstedt* [2001] and are given in Table 1, along with the grain size evolution parameters.

Table 1: Flow Law and Model Parameters

Symbol	Description	Value	Units
n_{disl}	dislocation creep exponent	4	dimensionless
n_{GBS}	GBS creep exponent	1.8	dimensionless
A_{disl}	dislocation creep prefactor (>259 K, ≤ 259 K)	3.8540e16, 5.0102e-13	$Pa^{-4}\,s^{-1}$
A_{GBS}	GBS creep prefactor (>259 K, ≤ 259 K)	7.4825e6, 4.9883e-18	$Pa^{-1.8}\,m^{1.4}\,s^{-1}$
Q_{disl}	dislocation creep activation energy (>259 K, ≤ 259 K)	180, 60	kJ/mol
Q_{GBS}	GBS creep activation energy (>259 K, ≤ 259 K)	192, 49	kJ/mol
m_{disl}	dislocation creep grain size exponent	0	dimensionless
m_{GBS}	GBS creep grain size exponent	1.4	dimensionless
Q_{gg}	activation energy for grain growth	42	kJ/mol
K_{gg}	grain growth rate constant	9.1520e-18	m^p
p	grain growth exponent	6.03	dimensionless
γ	average specific grain boundary energy	0.065	J/m^2
$\lambda_{disl}, \lambda_{GBS}$	fraction of work done by dislocation and GBS creep to change grain boundary area	0.01, 0.01	dimensionless
c	geometric constant	3	dimensionless

2.3 Effective Viscosity

Geodynamics models often make use of a rheology in the form of an effective viscosity. To attain this, I use Newton's law of viscous friction (formulated in terms of the second invariant of the stress and strain rate tensors):

$$\sigma_{\mathrm{II}} = 2\eta_{eff}\dot{\varepsilon}_{\mathrm{II}}, \tag{9}$$

where η_{eff} is the effective viscosity, $\sigma_{II} = \sqrt{1/2\sigma_{ij}'^{\,2}}$and $\varepsilon_{II} = \sqrt{1/2\varepsilon_{ij}'^{\,2}}$ are the second invariants of the stress and strain rate tensors, respectively. Indices *ij* imply a summation over each deviatoric component. I combine Eq. (9) with the flow laws (Eq. 7, 8) to compute the effective viscosity for each mechanism of the flow law (e.g., dislocation creep and GBS creep):

$$\eta_{eff_k} = A_k^{-\frac{1}{n_k}} d^{\frac{m_k}{n_k}} \dot{\varepsilon}_{\mathrm{II}}^{\frac{1-n_k}{n_k}} \exp\left(\frac{Q_k}{n_k RT}\right). \tag{10}$$

The terms are the same as in Eq. (8). Because the two creep mechanisms in my model may be active simultaneously, I take the harmonic average of both viscosities and implement this in my numerical model:

$$\eta_{eff_{total}} = \left[\frac{1}{\eta_{eff_{GBS}}} + \frac{1}{\eta_{eff_{disl}}}\right]^{-1}. \tag{11}$$

The term effective viscosity indicates that the viscosity is not an inherent material property for a non-Newtonian medium. If the stress exponent $n = 1$, the viscosity will be independent of strain rate. However, in the case of ice where $n \neq 1$, it is clear from Eq. (10) that the effective viscosity will depend on the strain rate. Because grain size affects the flow law for GBS, the overall local effective viscosity will be influenced by the evolution of grain size.

2.4 Numerical Implementation

To simulate ice flow, I use the two-dimensional particle-in-cell finite-difference MATLAB® code SiStER (Simple Stokes solver with Exotic Rheologies). SiStER is based on the approach of *Gerya* [2010] and was originally developed to model lithospheric and mantle deformation [*Olive et al.*, 2014; 2016]. Because SiStER is set up to handle visco-elasto-plastic deformation with non-Newtonian rheologies, it is readily adapted to model the deformation of ice. SiStER operates using a fully-staggered Eulerian grid (Figure 5) to discretize the conservation of mass (Eq. 12) and momentum (Eq. 13):

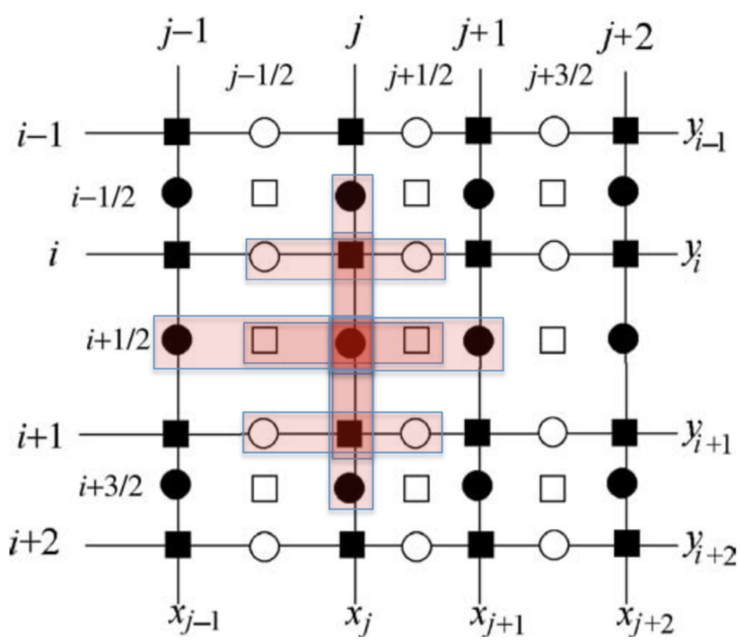

Figure 5. The fully-staggered grid used in SiStER for the discretization of the governing equations. The filled and empty circles are x- and y-velocity nodes, respectively, the filled and empty squares are shear and normal nodes, respectively [*Olive et al.*, 2016].

$$\nabla \cdot \vec{v} = 0 \tag{12}$$

$$\frac{\partial \sigma'_{ij}}{\partial x_j} - \frac{\partial P}{\partial x_i} + \rho g_i = 0, \tag{13}$$

where $\vec{v}$ is the velocity field, P is the pressure field, and ρg is the gravitational body force. Eq. (13) are the Stokes equations for creeping flows, where repeated indices imply summation.

The solution scheme for this model proceeds as follows: the conservation equations (Eqs. 12, 13) are solved on the nodes, giving the velocity field on the nodes. The velocity field is then interpolated onto Lagrangian markers, which are advected through the model domain according to this velocity field and a small timestep that satisfies the Courant condition. The Courant condition imposes a limit on the timestep such that the fastest moving markers are only advected a maximum of one-half grid cell forward, which ensures numerical stability in the advection scheme. Markers carry material properties, such as density, temperature, grain size, and therefore viscosity. After the markers are advected through one timestep, the material properties from the markers are interpolated back onto the Eulerian grid nodes in preparation for the next solve. A new velocity field is then computed, and the process repeats until a desired number of timestep iterations elapse (Figure 6).

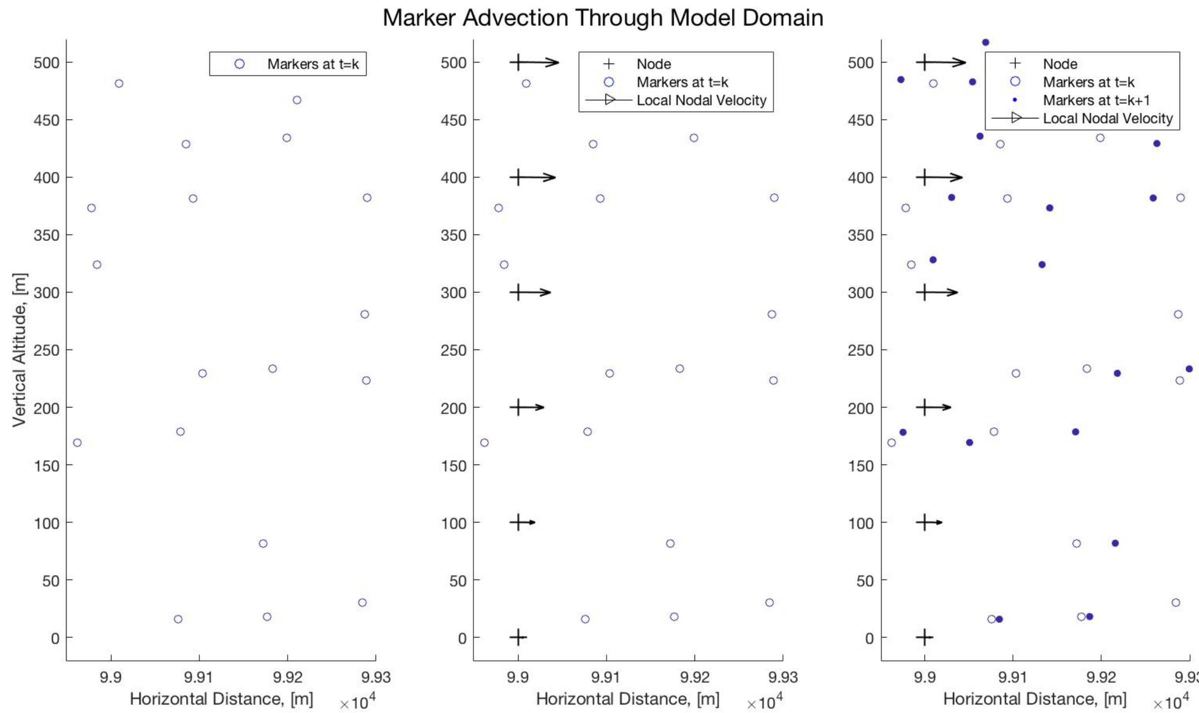

Figure 6. Sample marker-in-cell model process. From left to right: markers in the domain; those same markers as well as a velocity solution formulated on the nodes; the new marker positions after the velocity solution has been interpolated to the markers and the markers have been advected.

It is important to note here that grain size evolves at each timestep according to Eq. (5), and the evolution of grain size feeds back into the calculation of the viscosity to inform each velocity field solution.

2.5 Model Domain and Boundary Conditions

The model domain was chosen to reflect the well-studied "North Lake" Region [*Stevens et al.*, 2016] of the western margin of the GIS (Figure 7). To parameterize the surface topography across the region, I took ten elevation transects from Google Earth and fit a second-order polynomial to approximate these topography data (Figure 8).

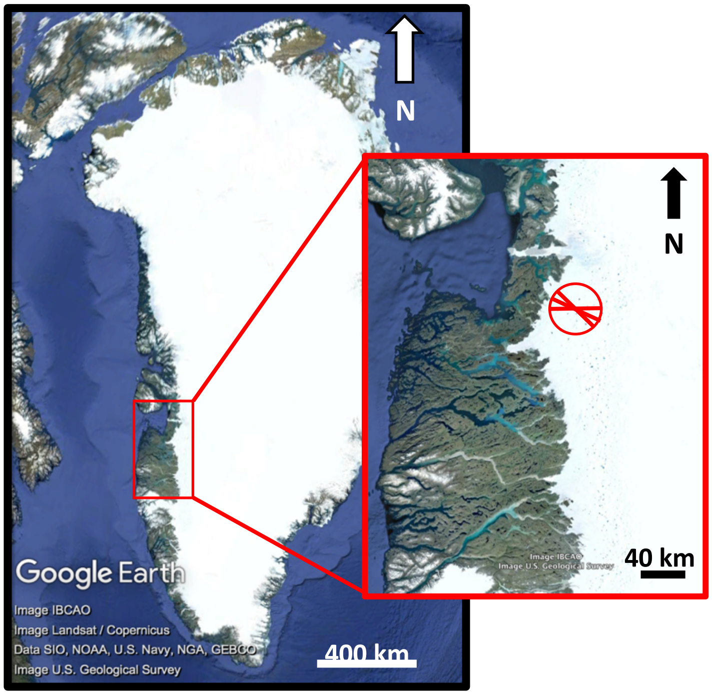

Figure 7. "North Lake" Region of the western margin of the GIS represented by my model. Located in the ablation zone of the GIS, the North Lake Region has been heavily studied for its abundance of meltwater lakes.

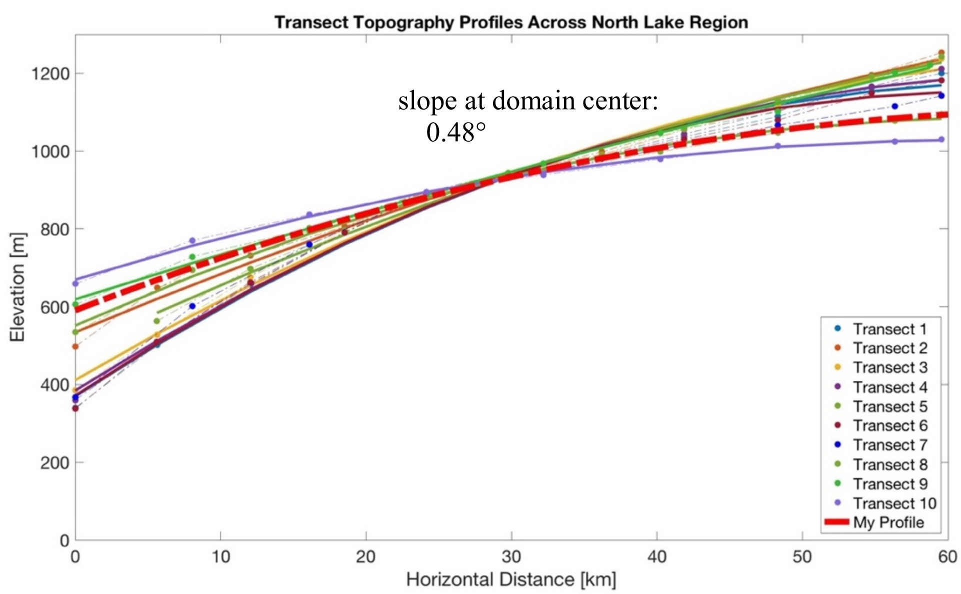

Figure 8. Topographic profiles across the North Lake Region of western Greenland taken from Google Earth. Red dashed curve shows the topographic profile implemented in my numerical model. Vertical dashed lines indicate the boundaries to the 30 km section of this profile used in my model.

The model domain is 30 km across, which represents the central half of the elevation profiles shown in Figure 8. The remaining 30 km of "unused" elevation data was gathered to better inform the shape of the topography for the model. Based on the imposed surface topography, ice flows from right to left across the domain (Figure 9), corresponding to east-to-west ice flow across the western margin of the GIS. In all calculations, I assume a spatially variable, but temporally constant, temperature distribution extrapolated from *Luthi et al.* [2002] throughout the ice sheet.

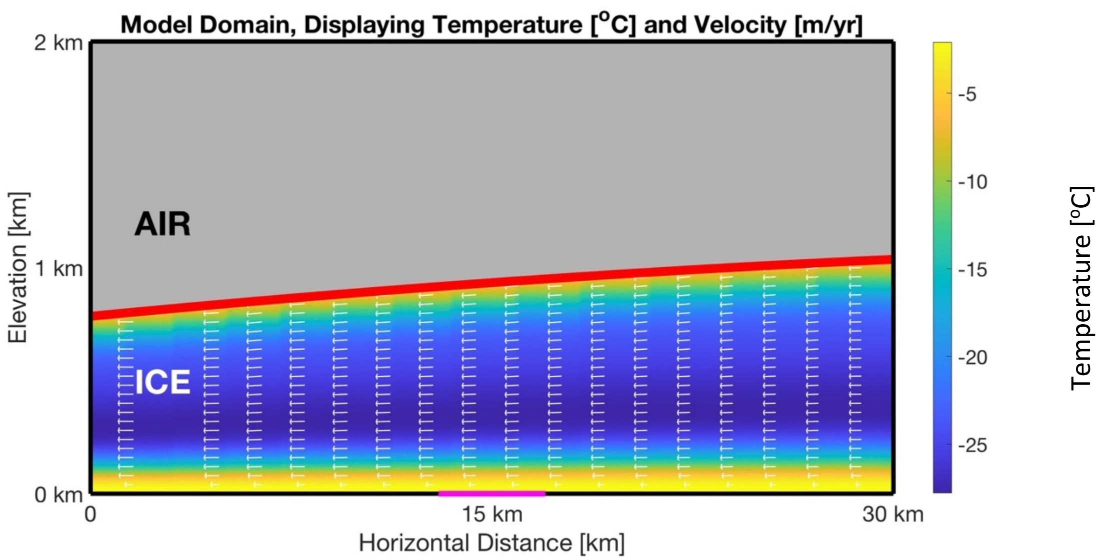

Figure 9. Model domain. Color map displays temperature (extrapolated/modified from *Luthi et al.* [2002]), which is a temporally-invariant profile through the ice, and the white arrows indicate velocity of ice flow, from right to left (roughly east to west). Note that air is grayed-out for simplicity. The temperature of the air matches the temperature of the surface of the ice.

Ice topography is temporally fixed in the model. This simplification is based on the assumption that accumulation and ablation are perfectly balanced across the domain. This simplification is discussed further in the Discussion section (§5).

The left and right boundary conditions are set as quasi-open boundaries. This is implemented through a near-zero horizontal velocity gradient across the boundaries and free-slip in the vertical direction, which allows ice to flow in/out of the domain freely according to the driving stress set by the topography. To simulate a free-surface of the ice, a “sticky” air is a layer is imposed above the ice with a viscosity higher (“stickier”) than real air, but much less than ice. The top boundary is set allow inflow/outflow of the “sticky” air to balance the difference between inflow and outflow at the vertical boundaries in order to maintain conservation of mass within the domain.

The basal boundary condition is the most important to this study. As a first order approximation for the seasonal presence of meltwater at the ice-bed interface, I implemented segments (patches) of free-slip along the basal boundary of the domain for three months out of every year. During these three summer months, the remainder of the boundary was held at a no-slip condition. During the nine remaining winter months I prescribed a no-slip condition across the entire basal boundary.

Each model simulation was run assuming a different number of free-slip basal patches, patch length, and separation between patches, for a total of 18 runs (Table 2). All simulations were initialized for 45 years with a no-slip condition at the bed before allowing the patch(es) of basal free slip to cycle on and off. This equilibration phase allowed grain size to reach near-equilibrium throughout the domain. Once the free slip patch(es) were activated, I ran each simulation for 25 additional years to investigate the effects that modifying the basal boundary condition has on the internal ice rheology.

Table 2. Patch geometries for GSE model simulations

Simulation	Total Slip Length [km]	Number of Patches	Length of Each Patch [km]	Separation Between Patches [km]
1	**2**	1	2	N/A
2	**2**	2	1	1
3	**2**	2	1	2
4	**2**	2	1	4
5	**4**	1	4	N/A
6	**4**	2	2	1
7	**4**	2	2	2
8	**4**	2	2	4
9	**4**	4	1	1
10	**4**	4	1	2
11	**4**	4	1	4
12	**8**	1	8	N/A
13	**8**	2	4	1
14	**8**	2	4	2
15	**8**	2	4	4
16	**8**	4	2	1
17	**8**	4	2	2
18	**8**	4	2	4

In addition to the simulations with GSE, I conducted two additional benchmark simulations: (1) with a constant (linear) surface slope and the Glen law rheology, and (2) a constant (linear) surface slope and constant temperature throughout the ice. These benchmark simulations are discussed in Section 3. In addition, I ran all basal patch geometries (Table 2) assuming an a fixed (temporally constant but spatially varying) equilibrium grain size profile (GSP) across the domain. Specifically, I allowed grain size to evolve for 45 years, as I did in the GSE runs, and then I held the grain size at that equilibrated profile, no longer allowing grain size to evolve, once the basal patch(es) were activated for the final 25 years of the simulations. These simulations thus make use of a grain size sensitive rheology, but did not allow grain size to evolve in time once the basal slip patch(es) were activated. These runs discussed further in the Results and Discussion sections (§4 and §5).

3. Model Benchmarks

The first benchmark simulation used the Glen law rheology under a constant (linear) surface slope and a narrow domain (Figure 10). I ran this setup in order to compare the performance of SiStER to a widely-accepted analytical solution for a 1-D column of ice deforming in simple shear [*Cuffey and Paterson*, 2010]. The horizontal velocity profile produced by the SiStER model agrees with that of the analytical solution to within 2% (Figure 11). This reinforced my confidence in the ability of the SiStER code to generate accurate results for gravity-driven flows appropriate for ice sheets.

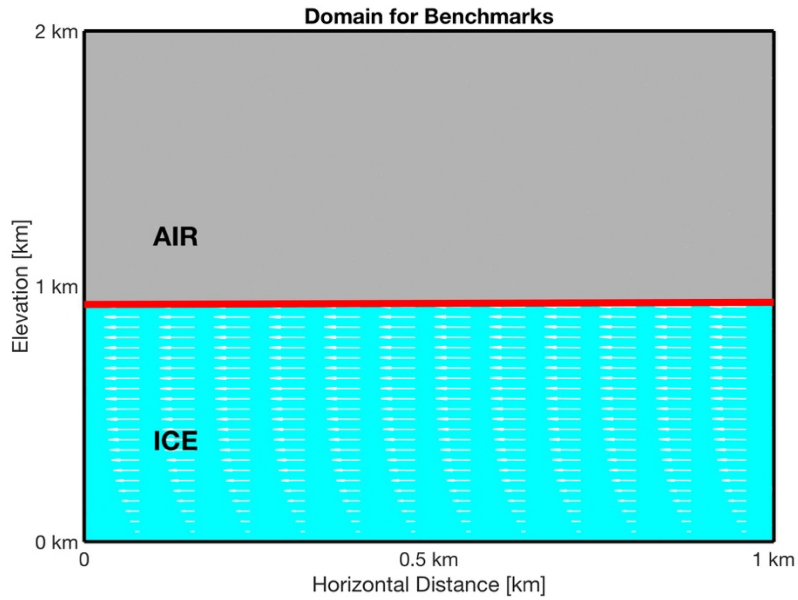

Figure 10. Domain used for benchmark model simulations. A linear topography with slope of 0.48° separates air (grey) from ice (blue). Ice flow is from right to left as depicted by white arrows.

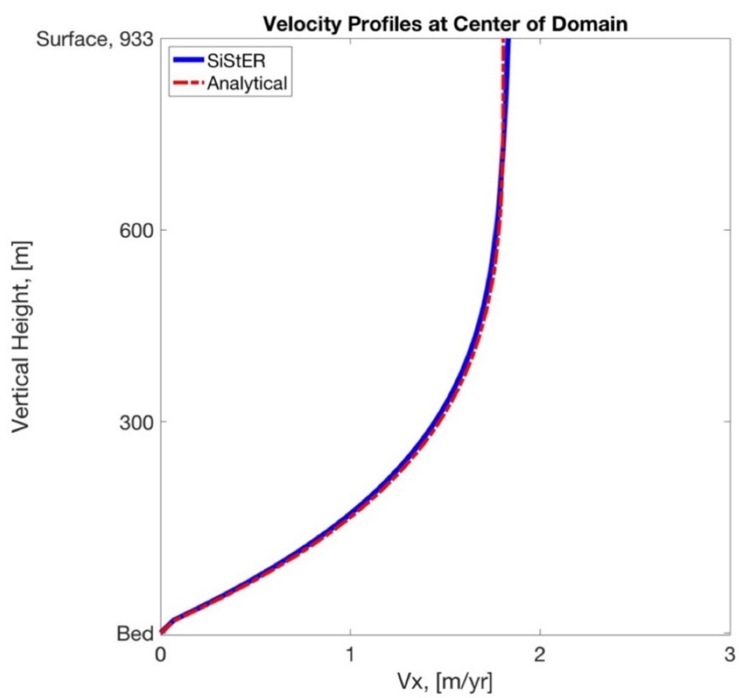

Figure 11. One-dimensional ice column horizontal velocity profile as a function of depth comparing the analytical solution (dashed red curve) and the SiStER modeled velocities (solid blue curve) assuming the Glen Flow law.

The second benchmark I carried out was to compare the results of the SiStER model under a linear surface slope and a fixed temperature of -10°C throughout the ice to the 1-D ice column results from *Behn et al.* [2021] (Figure 12).

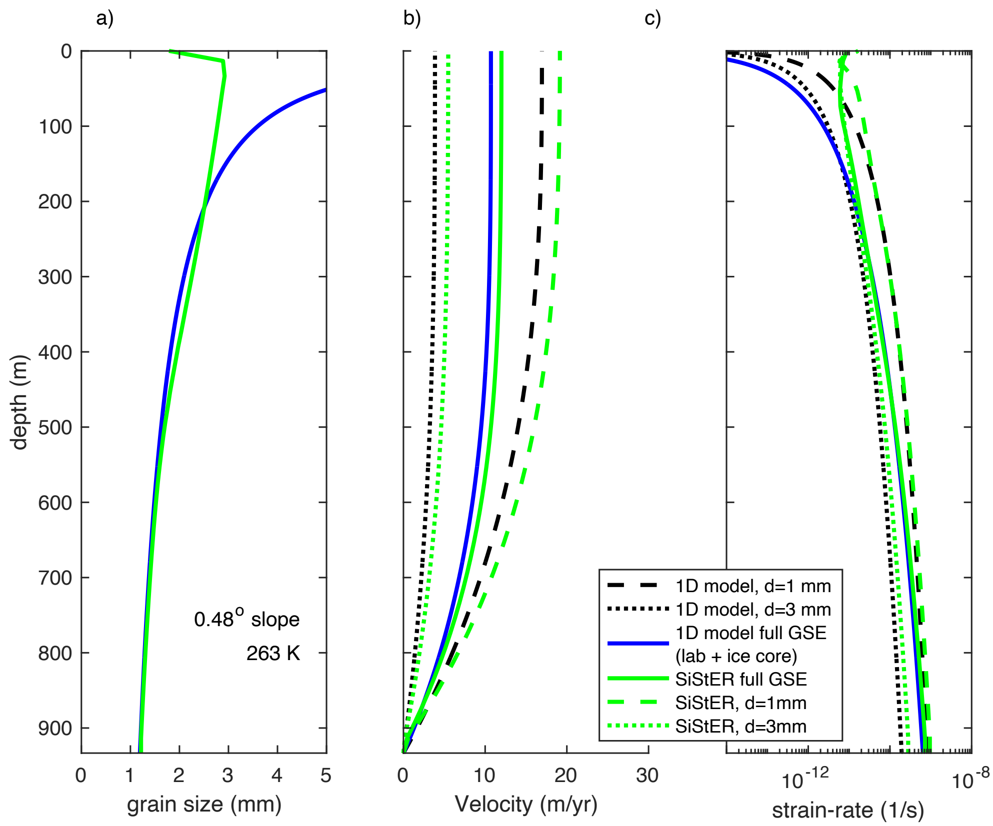

Figure 12. Modified from *Behn et al.* [2021]. Profiles with depth, comparing the SiStER code model results (green curves) to the 1D ice column results from *Behn et al.* [2021] (black and blue curves), showing **(a)** grain size, **(b)** velocity, and **(c)** strain rate.

While both models predict very similar grain sizes near the bed, there are slight differences between the 1-D model from *Behn et al.* [2021] and the 2-D SiStER model near the top of the domain. These discrepancies can largely be explained by the fact that the *Behn et al.* [2021] model allowed for grain size to equilibrate to a steady state at an infinite time. By contrast the 2-D SiStER simulations were run for only 25 years. Grain size equilibration times in the very slow straining ice near the surface are significantly longer than 25 years and grain size is still growing in this region in the SiStER simulations. Hence I interpret the differences in the simulations to reflect that the shallow grain sizes have not yet equilibrated. It is encouraging that the depth profiles of grain size, horizontal velocity, and strain rate below 800 m are comparable to the 1-D results. Further the surface velocities, which will be compared to GIS observations, are similar to ≤ 10% between simulations. This is a particularly informative benchmark because *Behn et al.* [2021] demonstrated the ability of the GSE model to accurately match grain size observations data from both the lab and from ice cores. Thus, I conclude that the SiStER model performs robustly against well-accepted benchmark simulations.

4. Results

In this section I present three key results of this study. The first is the effectiveness of the GSE model in capturing realistic horizontal winter and summer surface velocities on an annual timescale without the need to introduce an enhancement factor into the flow law (§4.1). The second result is the impact of seasonally-forced basal boundary perturbations on seasonal and inter-annual internal and basal ice grain size (§4.2). The third result is the inter-annual surface velocity response to the basal forcings (§4.3).

4.1 Winter and Summer Horizontal Velocity Profiles

As a first-order approximation for the basal boundary condition during winter when the ice is mostly frozen to the bedrock below, I imposed a no-slip condition across the ice-bed interface. Using the GSE rheology, I calculate winter velocity profiles as a function of depth (Figure 13a). The modeled winter velocities (green curve) are in good agreement with the observed surface velocities, which are between ~75 and ~85 m/yr for the region of the GIS simulated here (grey box, Figure 13a) [*Stevens et al.*, 2016]. This result is compared to the result obtained by using the unenhanced Glen law rheology in the same model setup. The Glen law rheology produces a winter velocity profile (solid blue curve, Figure 13a) with much slower surface velocities (2 m/yr) compared to the observed winter velocities. It is possible to reproduce the observed winter surface velocities by introducing an enhancement factor into the Glen law (i.e., by modifying the pre-factor, B, in Eq. 1). Specifically, to produce realistic winter surface velocities (dashed blue curve), I multiplied B by an enhancement factor of 45. Though the surface velocities produced by the GSE and the enhanced Glen Law rheologies is similar, the shape of the velocity profiles with depth differ significantly.

I next compared summer velocities to the range of observations assuming a single 4-km free slip patch centered in the middle of the model domain during the 3 summer months (Figure 13b). The choice of the free slip basal patch size was motivated by *Stevens et al.* [2015], who estimated the spatial extent of subglacial meltwater following a North Lake drainage event to be on the order of ~5 km. The GSE model again produces surface velocities that are within the observational range of *Stevens et al.* [2016]. However, as in the case of the winter velocities, the unenhanced Glen law rheology produces surface velocities that are well below the observational range. To test the enhanced Glen law, I introduce same enhancement factor that was effective in matching observations for the winter simulation. This produces a summer velocity profile with surface velocities well above the observational range. It would of course be possible to tune the enhancement factor for the summer simulation to match surface observations. By contrast, the GSE rheology predicts realistic winter and summer surface velocities without the need to introduce an ad hoc enhancement factor for each season independently. Further this suggests that grain size evolution captures the physical changes that occur within the ice sheet between the summer and winter seasons.

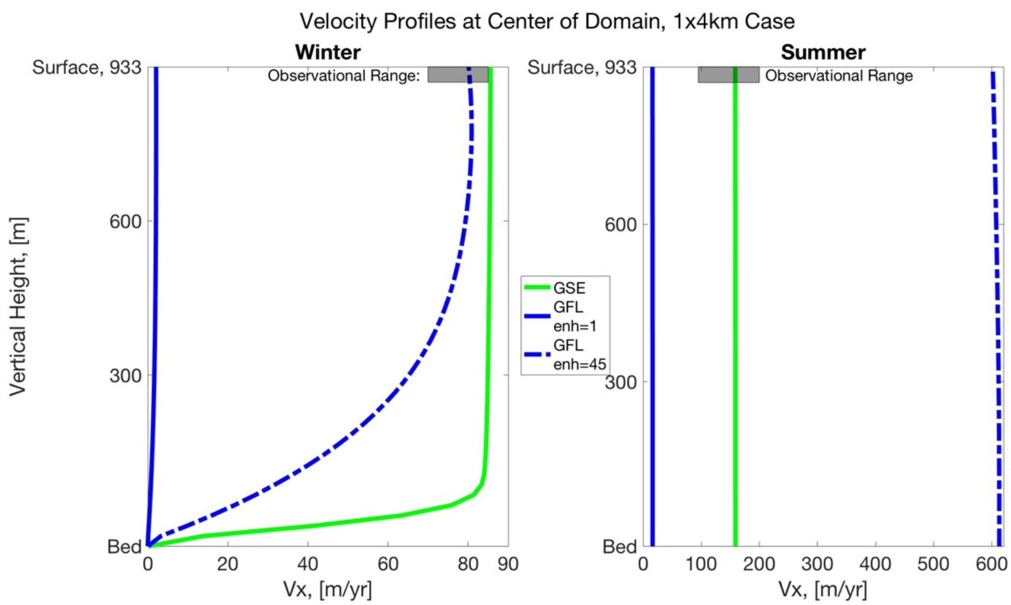

Figure 13. Profiles of the **(a)** winter and **(b)** summer horizontal velocities as a function of depth, analyzed at the center of the model domain shown in Figure 9. Blue curves show model velocities using the unenhanced (solid) and enhanced (dashed) Glen law rheology, green curves show model velocities using the GSE rheology. Observational ranges of surface velocities from *Stevens et al.* [2016] shown as grey boxes.

Applying the GSE rheology, I next explored the importance of varying the amount of free-slip imposed at the ice-bed interface. As expected, a larger region of free-slip results in faster surface velocities, and likewise slower surface velocities are found for smaller regions of free-slip. To demonstrate this trend, I averaged all summer velocities over the central 10 km of the surface across the 25 years and compared these values to the total basal decoupling length (Figure 14). In general, simulations with 4 km of free-slip across the 30-km domain best explain the observed summer velocities.

The geometry of the slip patch(es) also influences the average summer velocities, though to a lesser degree than the total amount of free slip. For the same total free slip length, a single patch (light blue symbols) produces the fastest average summer velocities, two patches (dark blue symbols) produce the second-fastest summer velocities, and four-patches (purple symbols) result in the slowest average summer velocities. Furthermore, for cases with multiple patches, larger separation between patches leads to slower average summer surface velocities. For example, the case with two 4-km free slip patches separated by 1 km (dark blue triangle) results in a faster average summer surface velocity than the case with two 4-km patches separated by 2 km (dark blue square). These trends are easiest to see by inspecting the 8 km total slip cases, but they hold for the 4 km and 2 km total slip cases as well. In general, patch geometry has a greater influence on summer velocities for greater lengths of free slip.

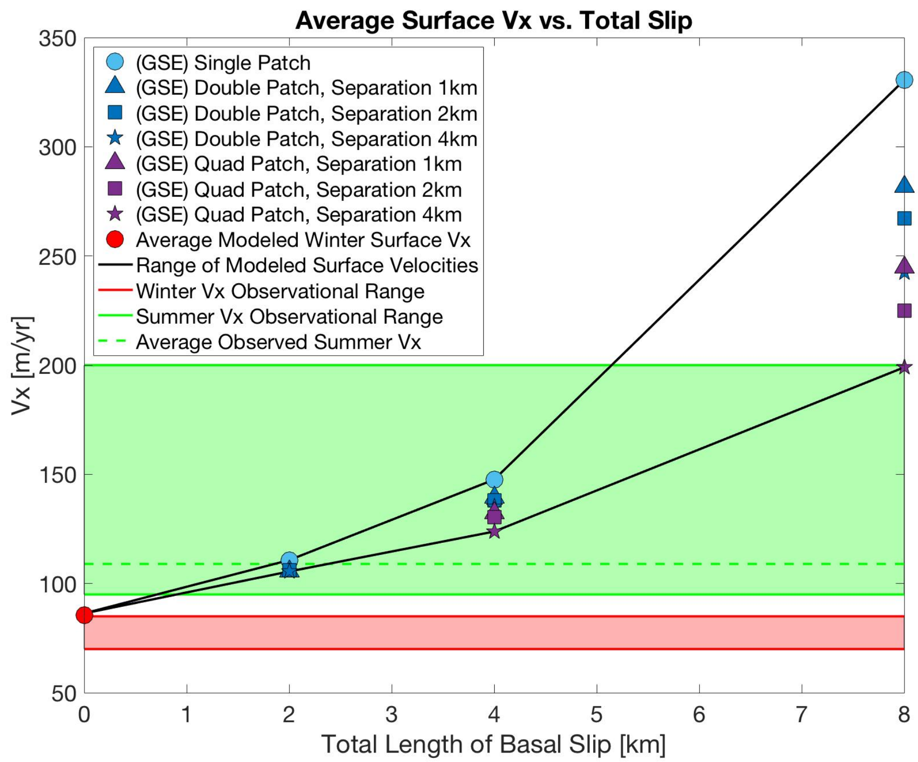

Figure 14. Average surface velocity versus total length of basal decoupling. Lightest blue markers show a single patch, darker blue represents a two-patch geometry, and purple indicates a four-patch system. The symbol indicates the separation between patches (triangle is 1 km separation, square is 2 km, and star is 4 km). Red and green shaded regions indicate ranges of observed surface velocity data from the western GIS, taken from *Stevens et al.* [2016]. The red circle indicates winter surface velocity from the model (no-slip at the bed).

4.2 Inter-Annual Variations in Ice Grain Size in Response to Seasonal Perturbations

When the basal boundary condition is set at no-slip (as during the winter months), there is a high shear stress, and therefore high workrate, applied on the basal ice. This results in small grain sizes, as the grain size reduction term (Eq. 4) dominates grain size evolution (Eq. 5) (Figure 15a). During the summer months, when a patch of free-slip is introduced at the bed, the reduction in shear stress (and hence workrate) over the patch leads to grain size evolution being dominated by the grain growth term (Eq. 3), while the ice near the edges of the free-slip patch experience stress concentrations that drive grain size reduction. These workrate perturbations propagate through the ice sheet, impacting the grain size evolution of the internal ice over the free-slip patch. The result is a region of permanent grain size reduction in the interior ice, especially on the upstream side of the patch, at the end of the 25-year model simulation time (as seen by the bluer internal ice in Figure 15b).

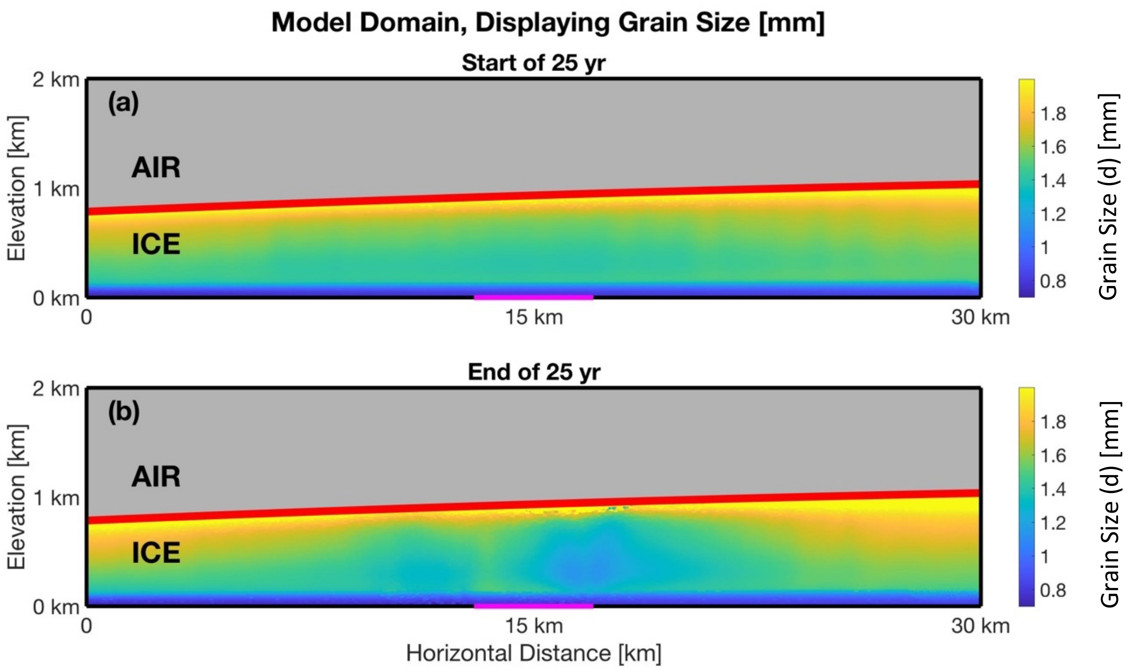

Figure 15. Grain size field at **(a)** the end of the 45-year no-slip spin-up period before free-slip patch is activated, and **(b)** at the end of the 25 years of annual basal perturbations. Results displayed for a simulation with a single 4-km patch. Pink line indicates location of patch.

To quantify and understand grain size evolution within the internal ice and at the bed, I analyzed the evolution of grain size in two horizontal profiles located 460 m and 0 m above the bed (Figure 16). The internal grain size at a depth of 460 m evolves slowly upon activation of the free-slip patch in the summer months. There is little change in the internal grain size during the course of the first summer season (orange profile, Figure 16a). Similarly, there is little difference after the first winter has elapsed (blue profile, Figure

16a). However, over the course of the 25 summer/winter cycles, a zone of permanent grain size reduction develops in the center of the domain, where grain size is reduced from ~1.6 mm to ~ 1.2 mm (green profile, Figure 16a). By contrast, permanent grain size reduction is not found in the basal ice (Figure 16b).

At the bed, grain size evolves on a seasonal timescale. Specifically, the grain size is reduced upstream and downstream of the patch and grows in the region interior to the patch during a single summer season (orange profile, Figure 16b). This is caused by the regions of enhanced workrate near the corners of the patch, which leads to enhanced grain size reduction. After the summer months, the entire basal boundary returns to a no-slip condition for the 9-month winter period. During this time, the basal grain size returns to the size exhibited before the patch was ever initiated (blue profile, Figure 16b). This trend continues year after year, and after the 25 years have elapsed, there is no long-term change to the basal grain size—i.e., the grain size at the end of the first winter and summer are identical to the grain size at the end of the 25th winter and summer (Figure 16b). Thus, the basal grain size evolves reversibly on a seasonal timescale, unlike the inter-annual timescale on which the internal grain size permanently evolves.

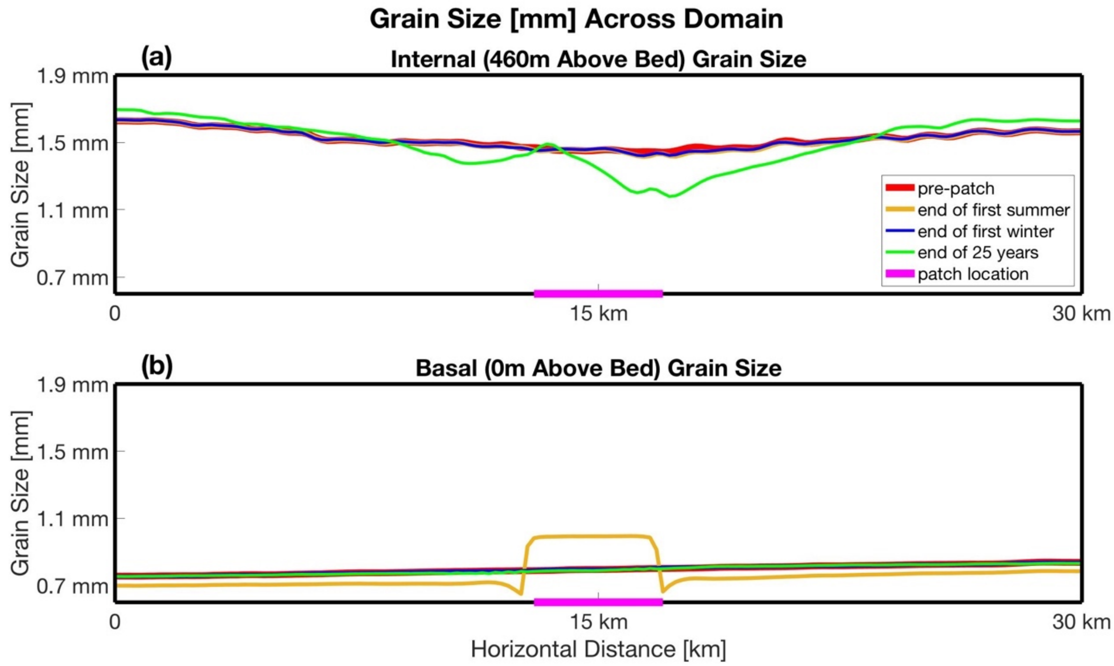

Figure 16. Seasonal changes to the **(a)** basal and **(b)** internal grain size for the single 4-km free-slip patch over a period of 25 years. The pink line shows the location of the free-slip patch. Red profile indicates grain size profiles at the end of the 45-year equilibration phase; orange profile represents the end of the first summer; blue represents the end of the first winter; and green represents the end of the final winter of the 25-year model simulation. There is no long-term change to the basal grain sizes, but there is permanent grain size reduction in the internal ice near the center of the domain.

I also conducted two simulations at two different spatially constant temperatures, one at –10°C and the other at –25°C. Similar to the cases above with variable temperature, I ran the constant temperature simulations for 25 years following a grain size equilibration period and analyzed grain size evolution at the start and end of each simulation (Figure 17).

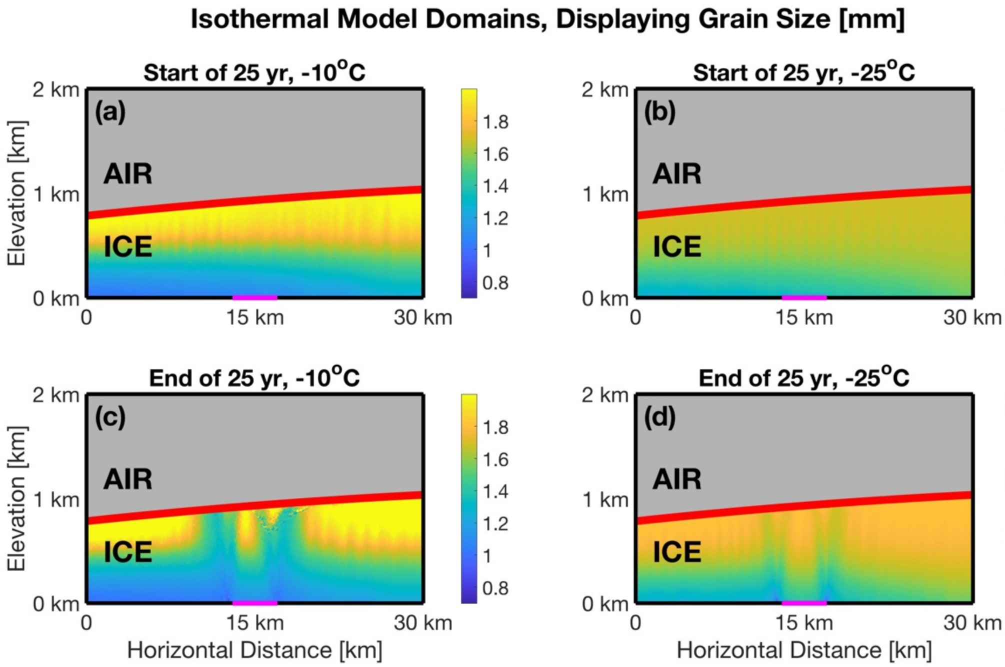

Figure 17. Grain size field before **(top row; a, b)** and after **(bottom row; c, d)** the 25-year simulations for isothermal cases set at -10°C **(left column; a, c)** and -25°C **(right column; b, d)**. Pink line indicates location of free-slip patch.

In the -10°C model, the internal grain size (blue curves, Figure 18a) is reduced significantly more than the internal ice in the -25°C model (black curves, Figure 18a). For the -10°C case, there is permanent grain size reduction throughout the interior of the ice. This implies that grain size reduction is more efficient than grain growth and that, similar to the variable temperature simulations, internal grain size does not "heal" seasonally. By contrast, there is very little grain size reduction and even some areas of grain growth in the interior ice for the -25ºC case. In the basal ice, the colder basal temperature in the –25°C simulation leads to permanent basal grain size reduction, with the most pronounced reduction at the margins of the patch (black curves, Figure 18b). By contrast, less reduction in basal grain sizes is observed in the –10ºC simulation (blue curves, Figure 18b).

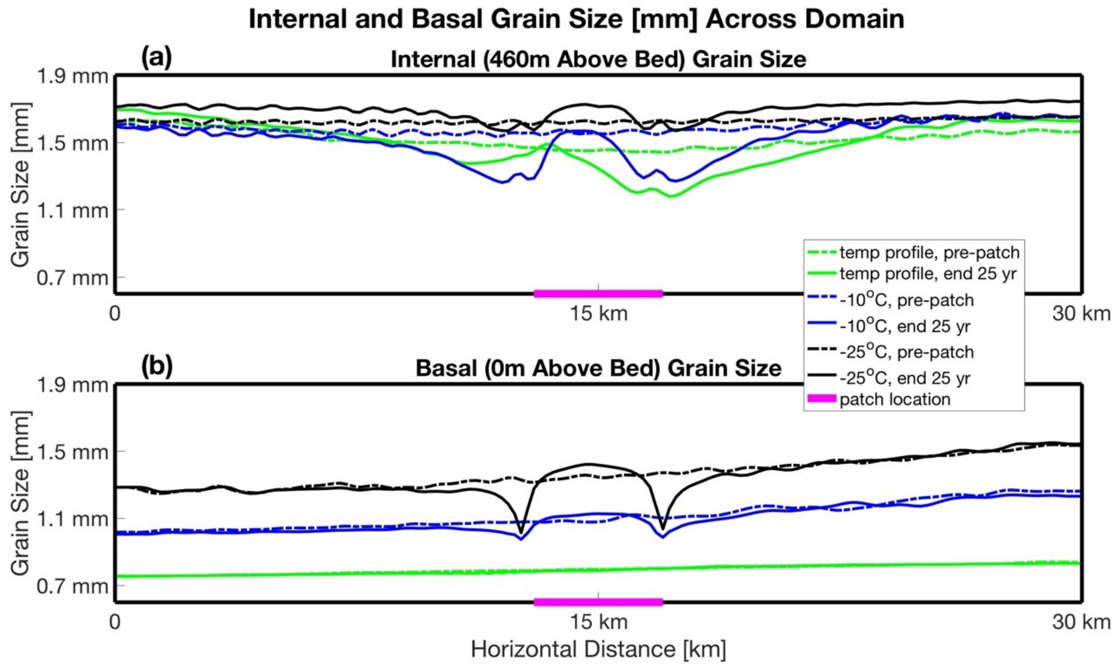

Figure 18. Grain size evolution of the **(a)** internal and **(b)** basal ice for isothermal models fixed at -10°C (blue profiles) and -25°C (black profiles). Grain size evolution from model with a realistic temperature profile shown for comparison (green profiles). Dashed lines indicate "pre-patch" equilibrium grain size profiles before the patch was turned on, solid lines indicate the grain size profile at the end of the 25-year model simulations.

4.3 Inter-Annual Surface Velocity Response

The permanent grain size reduction sustained over inter-annual timescales suggests that there may be corresponding long-term changes to ice deformation. To investigate this, I extracted the average surface velocity across the central 10 km of the domain during the beginning and end of each month from each of the 18 simulations (Figure 19).

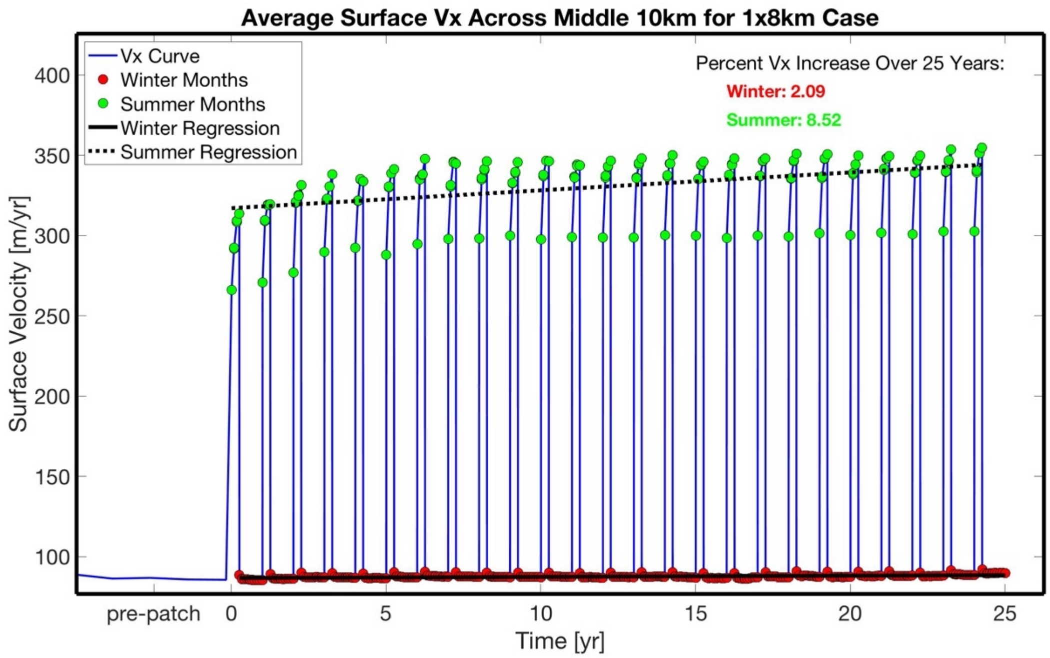

Figure 19. Average horizontal surface velocity across the middle 10 km of the domain for the single 8-km free slip patch model. Green dots indicate summer velocities, red dots indicate winter velocities, blue lines connect the months, showing the shape of the overall velocity curve.

It is clear that despite the variability in surface velocity, there is a trend toward higher velocities over the course of the 25-year simulation. This is particularly true for the summer velocities, which increase by ~8.5% over the course of the simulation. To further quantify this effect across all 18 simulations, I calculated a linear regression on the winter and summer velocities (solid and dashed black lines, respectively, Figure 19) for each 25-year run simulation. I then calculated the percent increase in winter and summer velocities according to these linear regressions (Figure 20a and b, respectively) for each of the 18 simulations.

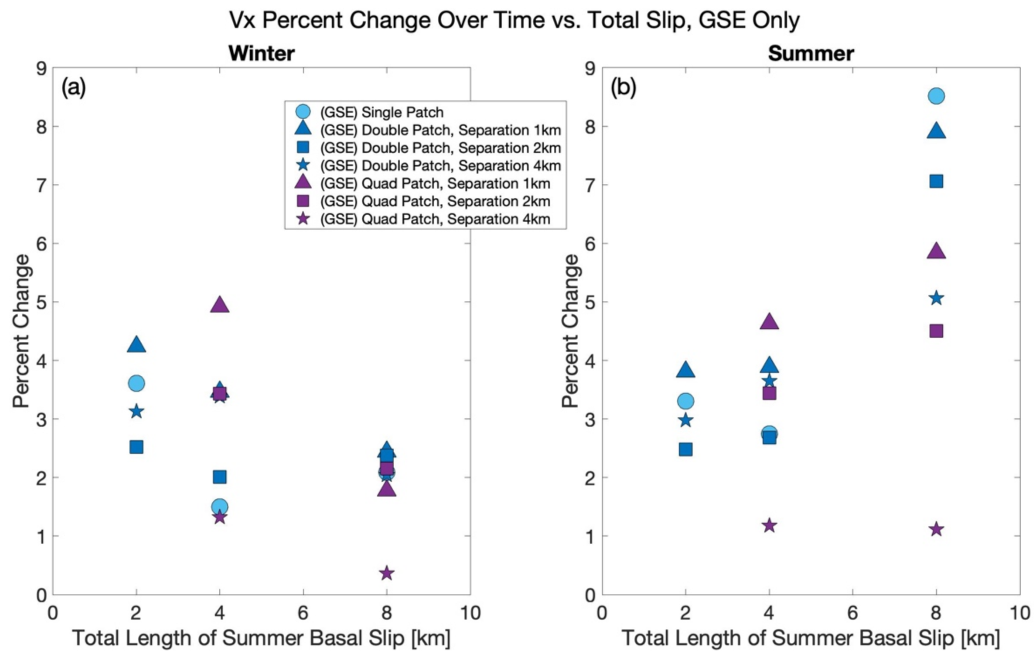

Figure 20. Percent change in winter (a) and summer (b) surface velocity over 25-year simulation run period for all 18 simulations.

The results from the winter velocity regressions show small velocity increases between 0–5%. The most consistent trend is that simulations with multiple patches separated by 1 km typically result in the greatest increase in winter velocity (Figure 20a). This trend holds for all total slip lengths except for 8 km, where the 4-patch system separated by 2 km produced a larger percent increase. Despite the lack of strong trends in the winter velocities, the summer velocity data produced more consistent and compelling evidence for a positive trend with time (Figure 20b). According to these results, summer surface velocities increase between ~1% and > 8% over the 25 years. In general, greater amounts of basal slip lead to a larger percent increase in summer surface velocities over the 25-year simulation. Additionally, multiple patch systems (two or four patches), typically exhibit a greater percent increase in summer surface velocity when the patches are closer together (e.g., the purple triangles plot above the purple squares, which plot above the purple stars in Figure 20b). This trend is likely because more patches result in more regions of enhanced grain size reduction due to the high concentration of stresses at patch edges. The trend holds for all but cases with 2 km of total slip.

To further test the importance of grain size evolution on the inter-annual velocity variations, I repeated the 18 simulations using a time-invariant grain size profile (as described in Methods section §2.5) (Figure 21). Nearly all of the grain size evolution (GSE) models (indicated by purple/blue symbols) produced higher percent increases in summer surface velocities than the corresponding fixed grain size profile (GSP) models (represented by orange/red symbols). The only case that breaks this trend is the four 1 km patches case (i.e., purple and dark red stars in the 4 km total slip column in Figure 21a). The change in winter surface velocities is also consistent with this trend, where most of the GSE models produce larger increases in surface velocity than the corresponding GSP models (Figure 21b). This indicates that long-term grain size reduction can lead to sustained weakening and thus faster ice velocities on decadal time scales.

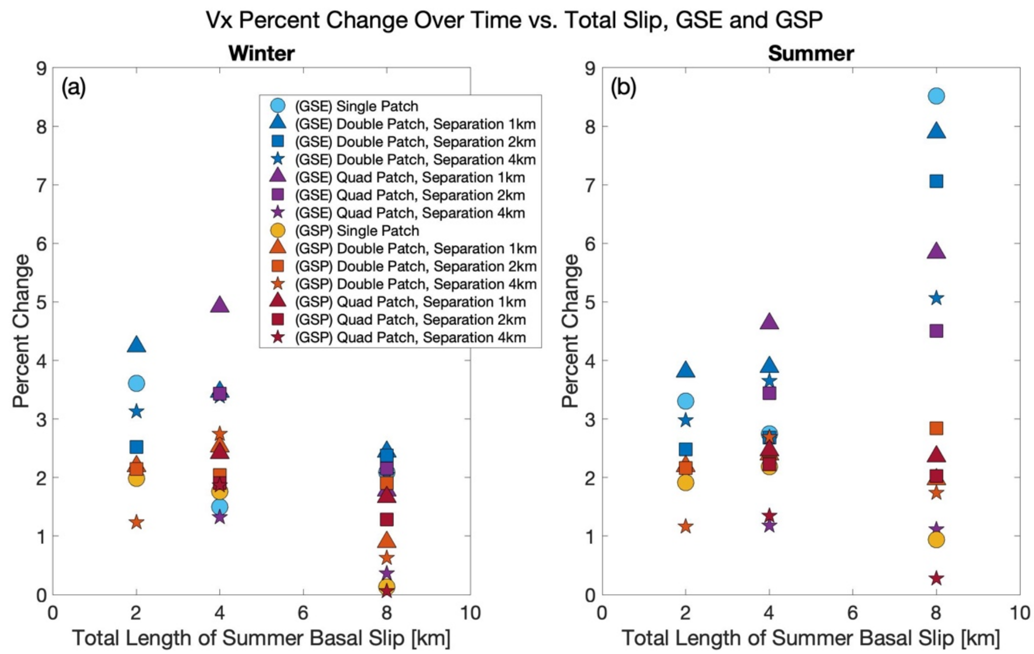

Figure 21. Percent change in winter (a) and summer (b) surface velocity over 25 year simulation period for all 18 GSE simulations (blue and purple symbols) as well as the 18 fixed grain size profile (GSP) runs (orange and red symbols). Nearly all the GSP models produced smaller summer surface velocity increases than their corresponding GSE models indicating that there is an enhanced surface velocity increase likely due to the permanent grain size reduction in the interior ice.

5. Discussion

In this section, I discuss the results of the study in the following order: the connection between the annual velocity trends and observation (§5.1), the effects of basal boundary condition perturbations on basal and internal grain size evolution on annual and interannual timescales (§5.2), and the long-term trends in surface velocity (§5.3).

5.1 Annual Velocity Trends

The relationship between surface velocity and patch geometry derived from my models (Figure 14) can be interpreted in terms of the observed surface velocities on the GIS [*Stevens et al*., 2016] and the hypothesis that seasonal changes in surface velocity reflect differences in the distribution of meltwater at the bed. In my simulations, greater amounts of free slip are assumed to correspond to greater amounts of meltwater at the bed [*Zwally*, 2002]. Further, the geometry of the slip patches may reflect the transition from distributed (pooled) to efficient (channelized) networks over the course of the summer season. In my simulations, a single patch could be considered analogous to a pooled subglacial meltwater network, which produces the fastest surface velocities. While multiple smaller patches for the same total free-slip area are analogous to a more channelized system, which produces slower surface velocities. These results imply that not only does the total amount of water beneath the ice matter, but the distribution geometry of the water also plays a role in surface velocity.

These results could be used as a guide to estimate the topology of basal decoupling beneath an ice sheet during different times of the year. For example, an early-summer surface velocity observation of 200 m/yr would imply that there was more than 4 km of total slip beneath the ice, regardless of the patch distribution, as the maximum surface velocity produced by 4 km of total slip was ~ 150 m/yr (light blue circle, 4 km column, Figure 14). An observation later in the summer of ~120 m/yr could then imply a similar maximum of 4 km of total slip at the bed, but that this slip might be organized in a more distributed geometry (purple star, 4 km column, Figure 14).

This interpretation is predicated upon the assumption that the free-slip-patch and no-slip conditions at the bed are realistic boundary conditions for the summer and winter, respectively. However, the use of free-slip patches to approximate the presence of lubricating water at the bed may not be physically realistic if some frictional coupling occurs even in areas of pooled meltwater. Rather, the use of no-slip and free-slip boundary conditions serve as end-member scenarios for the basal boundary. Future studies are needed to explore the effects of more realistic boundary conditions (e.g., reduced, but finite, basal shear stress) on the annual surface velocities.

5.2 Grain Size Response to Basal Forcing and Temperature

The evolution of the basal and internal grain size is similar for simulations with different patch geometries. For all cases in Table 2, the basal grain size fully "recovers" to its initial value during each winter season, while there is permanent grain size reduction in the interior ice. I hypothesize that this is largely due to the temperature profile assumed for ice sheet. In the cases using a realistic ice sheet temperature profile [*Luthi et al.*, 2002], the basal ice is held at a temperature near the melting point (~ –2°C), while the internal ice is much colder (~ –25°C) (Figure 9). Because the rate of grain growth is inversely proportional to temperature, warmer temperatures in regions of high workrate such as the basal ice facilitates more rapid grain growth. This helps to explain the recovery of the reduced grain sizes in the basal ice surrounding the free-slip patch during the winter months. Immediately above the patch, the reintroduction of no-slip across the bottom boundary in the winter increases the work rate compared to the summer months, which causes grain size to decrease back to its equilibrium state (blue profile, Figure 16b). Thus, my simulations suggest that basal ice may not experience long-term perturbations in grain size due to annual cycles in summer vs. winter variations in basal coupling.

In the internal ice, the colder temperatures suppress grain growth and grain size does not recover as rapidly. This ultimately leads to permanent grain size reduction in the internal ice. This reasoning is further supported by the two additional constant temperature simulations (Figure 17). These simulations, which demonstrate that colder basal temperatures encourage permanent grain size reduction, are consistent with the trend in the GSE model where the colder internal temperatures likely prevent the seasonally-reduced grain sizes from recovering back to their pre-patch equilibrium state (Equation 5). In the simulations with variable temperature, the observation that basal grain size experiences seasonal cycles in reduction and full recovery is likely due to a close balance between the grain growth and grain reduction term (Equation 5).

The observations that internal grain size is also dependent on temperature (Figure 18a) may be explained by the fact that strain rate is also temperature dependent, where warmer temperatures encourage lower viscosities, and thus higher strain rates. This in turn leads to grain size reduction balancing grain growth during the winter months due to the higher work rates (Eq. 5), and therefore the internal ice in this simulation is not able to fully recover to its pre-patch equilibrium state in the -10ºC, whereas grain size is able to recover more fully in the -25ºC case. Because I see a permanent grain size reduction in the simulations using a realistic temperature-depth profile, the lack of internal grain size reduction in the -25ºC case is likely due to the impact of the spatially-constant temperature field on the grain size evolution. These results further confirm that the temperature profile is an important parameter in controlling grain size evolution on both seasonal and inter-annual timescales.

With the realistic temperature profile as applied in all other simulations (Figure 9), the basal temperature is warm enough for the basal grain size to undergo no permanent changes (green curves, Figure 18b), while the internal ice experiences a permanent grain size reduction (green curves, Figure 18a). It is important to note here that the viscosity of ice is proportional to grain size, where a reduction in grain size leads to a subsequent reduction of ice viscosity (Equation 10). For example, based on the simulation using a single 8-km patch seasonally over 25 years, a ~20% reduction of internal grain size (from ~1.5 mm to ~ 1.2 mm) corresponds to a GBS viscosity reduction of ~16% (Equation 10). Thus, the reduced grain size of the internal ice results in a type of damage to the ice viscosity, and thus could play a role in large-scale ice dynamics. In addition to regions experiencing variable basal boundary conditions, permanent changes in grain size and viscosity could be important near shear margins where ice is incorporated into ice streams.

5.3 Long-Term Surface Velocities

The trend of increasing surface velocities over time (Figure 21) is likely caused by the inter-annual grain size reduction that occurs in response to the seasonal perturbations in the basal boundary condition. Specifically, the more pronounced increase in surface velocities with GSE as compared with the fixed grain size profile (GSP) simulations supports the conclusion that seasonal perturbations at the ice-bed boundary condition may lead to inter-annual internal damage and reduction of ice viscosity, which may be reflected in long-term changes to ice dynamics. These velocity increases of < 10% over 25 years is small, but non-negligible, compared to observations of GIS surface velocity doublings over 10 years [*Rignot & Kanagaratnam*, 2006]. Further quantification of this is necessary to determine the functional relation between inter-annual grain size evolution and surface velocity.

6. Conclusions and Future Directions

There are three main conclusions from this work. The first is the high degree of effectiveness of using a GSE-sensitive rheology [*Goldsby & Kohlstedt*, 2001] in ice sheet modeling. The GSE rheology produces realistic winter and summer velocities, implying that models implementing this rheology may be able to effectively capture the dynamics of grounded ice sheets without the need to introduce different enhancement factors into the Glen flow law. One observation that would be useful to further test this claim would be to compare the velocity profile with depth as computed by the model (Figure 13a) with ice core observations. The shape of the velocity curve produced by an enhanced Glen law rheology differs significantly from that from the GSE model. Such a test would require knowledge of the local vertical velocity profile, which could be determined by tiltmeters [e.g., *Harper et al.*, 2001], as well as temperature and grain size with depth in order to constrain and directly compare the model to the observations.

The second conclusion from this work is that the grain size of the internal ice changes on an inter-annual timescale in response to the seasonally-periodic introduction of free-slip patch(es) at the ice-bed interface. In particular, much of the internal ice experiences net grain size reduction over inter-annual time scales, effectively weakening the ice. This sustained internal ice weakening can lead to enhanced summer surface velocity increases across time. Further quantification of this relationship between internal grain size reduction, temperature, and surface velocity changes is needed. Because grain size evolution model is sensitive to temperature, it would be useful to have direct observations of vertical co-variations in grain size and temperature in order to inform and interpret the grain size evolution.

The third conclusion from this project is that 2-D models with periodic basal boundary conditions can be used to provide bounds on the amount of decoupling of the ice-bed interface, and therefore the amount of water present at the bed, by comparing the modeled and observed surface velocities. The variation in summer surface velocity as a function of both total basal slip and patch geometry under the free-slip and no-slip assumptions (Figure 14) can serve as a proxy for a first-order approximation of the amount and orientation of basal decoupling beneath a grounded ice sheet. Specifically, I find that free-slip over 6–25% of the bed most closely reproduces the observed summer velocities of 100–200 m/yr. A logical next step for this work is to introduce more realistic basal boundary conditions including frictional shear patches and/or basal topography, as well as an ice sheet surface that can evolve in response to ablation/accumulation. Such improvements will allow for even more robust models to link changes in basal processes to ice sheet dynamics.

References

Alley, R. & Woods, G. (1996). Impurity influence on normal grain growth in the GISP2 ice core, Greenland. *Journal of Glaciology*, 42, 255-260.

Alley, Richard. (1992). Flow-law hypotheses for ice-sheet modeling. *Journal of Glaciology*, 38. 245-256.

Alley, R., Perepezko, H. and Bentley, C. (1986). Grain growth in polar ice: 1. Theory, *Journal of Glaciology*, 32(112), 415–424.

Austin, N. and Evans, B. (2009). The kinetics of microstructural evolution during deformation of calcite. *J. Geophys. Res.*, 114(B9), B09402.

Austin, N. J. and Evans, B.: Paleowattmeters (2007). A scaling relation for dynamically recrystallized grain size. *Geol.*, 35(4), 343.

Behn, M. D., Goldsby, D. L., and Hirth, G. (2021). The role of grain size evolution in the rheology of ice: implications for reconciling laboratory creep data and the Glen flow law. *The Cryosphere*, 15, 4589–4605.

Cuffey, K. M. and Paterson, W. S. B. (2010). Physics of Glaciers, 4th ed., *Elsevier*, Amsterdam.

Das, S. B., Joughin, I., Behn, M. D., Howat, I. M., King, M. A., Lizarralde, D., et al. (2008). Fracture propagation to the base of the Greenland Ice Sheet during supraglacial lake drainage. *Science,* 320, 778–781.

Doyle, S.H., A. L. Hubbard, C.F. Dow, G.A. Jones, A. Fitzpatrick, A. Gusmeroli, B. Kulessa, K. Lindback, R. Pettersson, and J.E. Box (2013). Ice tectonic deformation during the rapid in situ drainage of a supraglacial lake on the Greenland ice sheet. *Cryosphere*, 7(1), 129-140.

Faria, S. H., Weikusat, I. and Azuma, N. (2014a). The microstructure of polar ice. Part I: Highlights from ice core research, *J. Struc. Geol.,* 61, 2–20.

Fountain, Andrew G., Walder, Joseph S. (1998). Water flow through temperate glaciers. *Reviews of Geophysics*, 36 (3). 299-328.

Geosciences and Environmental Change Science Center (2000). Grains in an ice thin-section., Image, https://www.usgs.gov/media/images/grains-ice-thin-section

Gerya, T. (2010). Introduction to Numerical Geodynamic Modelling. xvii 345. Cambridge University Press. *Geological Magazine, 149*(1), 174-174.

Glen, J. W. (1952). Experiments on the Deformation of Ice. *Journal Of Glaciology*, 2(12), 111–114.

Glen, J. W. (1955). The creep of polycrystalline ice. *Proceedings of the Royal Academy of London Series,* 228(1175), 519–538.

Goldsby, D. L. and Kohlstedt, D. (2001). Superplasticdeformation of ice: Experimental observations*, J. Geophys. Res.,* 106(B6), 11,017–11,030.

Gow, A. J. and Williamson, T. (1976). Rheological implications of the internal structure and crystal fabrics of the West Antarctic ice sheet as revealed by deep core drilling at Byrd Station, *GSA Bull.,* 87(12), 1665–1677.

Gow, A. J., Meese, D. A., Alley, R. B., Fitzpatrick, J. J., Anandakrishnan, S., Woods, G. A. and Elder, B. C. (1997). Physical and structural properties of the Greenland Ice Sheet Project 2 ice core: A review, *J. Geophys. Res.,* 102(C12), 26559–26575.

Hall, C. E. and Parmentier, E. M.(2003). Influence of grain size evolution on convective instability, *Geochem. Geophys. Geosys.,* 4(3).

Hanna, E., Navarro, F., Pattyn, F. et al (2013). Ice-sheet mass balance and climate change. *Nature* 498, 51–59.

Harper, J. T., Humphrey, N. F., Pfeffer, W. T., Huzurbazar, S. V., Bahr, D. B., and Welch, B. C. (2001). Spatial variability in the flow of a valley glacier: Deformation of a large array of boreholes, *J. Geophys. Res.*, 106(B5), 8547– 8562.

Hewitt, Ian. (2013). Seasonal changes in ice sheet motion due to melt water lubrication. *Earth and Planetary Science Letters*. s 371–372. 16–25.

Joughin, I., Das, S. B., Flowers, G. E., Behn, M. D., Alley, R. B., King, M. A., Smith, B. E., Bamber, J. L., van den Broeke, M. R., and van Angelen, J. H. (2013). Influence of ice-sheet geometry and supraglacial lakes on seasonal ice-flow variability, *The Cryosphere*, 7, 1185–1192.

Lüthi, M., Funk, M., Iken, A., Gogineni, S. and Truffer, M. (2002). Mechanisms of fast flow in Jakobshavn Isbrae, West Greenland: Part III. Measurements of ice deformation, temperature and cross-borehole conductivity in boreholes to the bedrock, *J. Glaciol.,* 48(162), 369–385.

Millstein, J., Minchew B., Pegler, S. (Preprint, Compiled 2021). Ice Viscosity Is More Sensitive to Stress Than Commonly Assumed, *Nature Communications Earth & Environment*.

Nieh, T. G., Wadsworth, J. and Sherby, O. D. (1997). *Superplasticity in Metals and Ceramics, 1st ed., Cambridge University Press.*

Olive, J-A.O, Mark D. Behn, Eric Mittelstaedt, Garrett Ito, Benjamin Z. Klein (2016). The role of elasticity in simulating long-term tectonic extension, *Geophysical Journal International*, Volume 205, Issue 2, Pages 728–743.

Olive J.-A., Behn, M.D., Malatesta, L.C. (2014). Modes of extensional faulting controlled by surface processes, *Geophys. Res. Lett.* 41,19, 6725, 6733.

Paterson, W. S. B. (1983). Deformation within polar ice sheets: An analysis of the Byrd Station and Camp Century borehole-tilting measurements, *Cold Reg. Sci. Tech*., 8(2), 165–179.

Poirier, J.-P. (1985). Creep of Crystals: High-Temperature Deformation Processes in Metals. *Ceramics and Minerals, 1st ed., Cambridge University Press.*

Pritchard, H., Arthern, R., Vaughan, D. et al. (2009). Extensive dynamic thinning on the margins of the Greenland and Antarctic ice sheets. *Nature* 461, 971–975 (2009).

Ranganathan, M., Minchew, B., Meyer, C., Peč, M. (2021). Recrystallization of ice enhances the creep and vulnerability to fracture of ice shelves. *Earth and Planetary Science Letters,* Volume 576.

Rignot, Eric, and Pannir Kanagaratnam (2006). Changes in the Velocity Structure of the Greenland Ice Sheet. *Science*, vol. 311, no. 5763, pp. 986–90.

Roessiger, J., Bons, P. D., Griera, A., Jessell, M. W., Evans, L., Montagnat, M., Kipfstuhl, S., Faria, S. H. and Weikusat, I. (2011). Competition between grain growth and grain-size reduction in polar ice, *J. Glaciol.,* 57(205), 942–948.

Schoof, C (2010). Ice-sheet acceleration driven by melt supply variability. *Nature* 468, 803–806.

Shepherd, A., Ivins, E. R., A, G., Barletta, V. R., Bentley, M. J., Bettadpur, S., Briggs, K. H., Bromwich, D. H., Forsberg, R., Galin, N., Horwath, M., Jacobs, S., Joughin, I., King, M. A., Lenaerts, J. T. M., Li, J., Ligtenberg, S. R. M., Luckman, A., Luthcke, S. B. et al. (2012). A reconciled estimate of ice-sheet mass balance. *Science,* 338(6111), 1183–1189.

Stevens, Laura & Behn, Mark & Das, Sarah & Joughin, Ian & Noël, Brice & Van den Broeke, Michiel & Herring, T.. (2016). Greenland Ice Sheet flow response to runoff variability. *Geophysical Research Letters*, 43.

Stevens, L., Behn, M., McGuire, J. et al. (2015). Greenland supraglacial lake drainages triggered by hydrologically induced basal slip. *Nature* 522**,** 73–76 (2015).

Van den Broeke, Michiel & Bamber, Jonathan & Ettema, Janneke & Rignot, E. & Schrama, Ernst & Berg, W.J. & Meijgaard, Erik & Velicogna, Isabella & Wouters, Bert. (2009). Partitioning Recent Greenland Mass Loss. *Science*, 326. 984-6.

Weertman, J. (1983). Creep deformation of ice. *Ann. Rev. Earth Planet. Sci.*

Zwally HJ, Abdalati W, Herring T, Larson K, Saba J, Steffen K. (2002). Surface melt-induced acceleration of Greenland ice-sheet flow. *Science*. 2002 Jul 12;297(5579):218-22.